A sound horizon-free measurement of H_0 in DESI 2024

Journal of Cosmology and Astroparticle Physics
An IOP and SISSA journal

Received: *November 26, 2024*
Accepted: *May 12, 2025*
Published: *June 17, 2025*

A sound horizon-free measurement of H_0 in DESI 2024

E.A. Zaborowski et al.
Full author list at the end of the paper

E-mail: zaborowski.11@osu.edu

Abstract: The physical size of the sound horizon at recombination is a powerful source of information for early-time measurements of the Hubble constant H_0, and many proposed solutions to the Hubble tension therefore involve modifications to this scale. In light of this, there has been growing interest in measuring H_0 independently of the sound horizon. We present the first such measurement to use data from the Dark Energy Spectroscopic Instrument (DESI), jointly analyzing the full-shape galaxy power spectra of DESI luminous red galaxies, emission line galaxies, quasars, and the bright galaxy sample, in a total of six redshift bins. Information from the sound horizon scale is removed from our constraints via a rescaling procedure at the power spectrum level, with our sound horizon-marginalized measurement being driven instead primarily by the matter-radiation equality scale. This measurement is then combined with additional sound horizon-free information from *Planck*+ACT CMB lensing, uncalibrated type Ia supernovae, and the DESI Lyman-α forest. We agnostically combine with the DESY5, Pantheon+, and Union3 supernova datasets, with our tightest respective constraints being $H_0 = 66.7^{+1.7}_{-1.9}$, $67.9^{+1.9}_{-2.1}$, and $67.8^{+2.0}_{-2.2}\,\mathrm{km\,s^{-1}\,Mpc^{-1}}$. This corresponds to a sub-3% sound horizon-free constraint of the Hubble constant, and is the most precise measurement of its kind to date. Even without including information from the sound horizon, our measurement is still in 2.2-3.0σ tension with SH0ES. Additionally, the consistency between our result and other measurements that *do* rely on the sound horizon scale provides no evidence for new early-Universe physics (e.g. early dark energy). Future DESI data releases will allow unprecedented measurements of H_0 and place strong constraints on models that use beyond-ΛCDM physics to ameliorate the Hubble tension.

Keywords: cosmological parameters from LSS, power spectrum, redshift surveys, physics of the early universe

ArXiv ePrint: 2411.16677

https://doi.org/10.1088/1475-7516/2025/06/020

JCAP06(2025)020

Contents

JCAP06(2025)020

1 Introduction

The Hubble tension (see [1] for a review) is one of the most pressing issues in cosmology. The Hubble constant H_0 parameterizes the expansion rate of the Universe, and in particular there is a $\sim 5\sigma$ discrepancy between the local distance ladder measurement of H_0 by the SH0ES collaboration [2], and the measurement reported by the *Planck* collaboration [3] using the cosmic microwave background (CMB). This difference could arise either because of unrealized systematic errors in one or both measurements, or due to new physics beyond the standard Λ Cold Dark Matter (ΛCDM) model of cosmology (see [4] for an extensive review of possible solutions to the Hubble tension, and e.g. [5–7] for more recent investigations of some systematics). Many high-redshift/early-time H_0 constraints, such as those from the CMB (e.g. [3, 8]) or from baryon acoustic oscillations (BAO; e.g. [9–14]), derive a significant amount of information from the physics of recombination and the sound horizon distance at

the time of recombination.[1] The sound horizon is a standard ruler that, once calibrated, can be used to infer H_0 from the relevant features in these datasets (see section 2). Because of this, many solutions to the Hubble tension that rely on modifications to physics to decrease the physical size of the sound horizon have been proposed [17]. This includes, among others: early dark energy (EDE) [18–20], additional light degrees of freedom [21, 22] or new interactions between them [23–25], and reduction of the sound speed in the photon-baryon plasma prior to decoupling [17].

For this reason, there has been growing interest in measuring H_0 independently of the sound horizon scale [26–29]. In [26] it was proposed to measure H_0 using the gravitational lensing of the CMB, which is not sensitive to the sound horizon scale, but rather to the wavenumber $k_{\rm eq}$ corresponding to the comoving horizon size at the epoch of matter-radiation equality (see section 2). The precision of this measurement can then be improved by combining with additional information on the matter density $\Omega_{\rm m}$, which they sourced from uncalibrated type Ia supernovae (SNe Ia). A recent application of this method by [30] using CMB lensing data from the Atacama Cosmology Telescope (ACT; [31, 32]) and *Planck* [33–36], combined with galaxies from the unWISE catalog [37] and uncalibrated supernovae from the Pantheon+ dataset [38], resulted in a precise sound horizon-free measurement of $H_0 = 64.3^{+2.1}_{-2.4}\,\mathrm{km\,s^{-1}\,Mpc^{-1}}$. Others have measured H_0 without the sound horizon through a direct measurement of $k_{\rm eq}$, via the turnover scale of the matter power spectrum [39]. In [40], a similar measurement of the horizon size at matter-radiation equality was proposed via the zero-crossing scale of the matter correlation function. Recently, [41] demonstrated that H_0 can be derived from measurements of cosmological energy densities without including information from the sound horizon scale.

Galaxy surveys provide one of the most promising avenues to measure H_0 without the sound horizon. As remarked in [27], a 3D galaxy survey can typically probe a much larger number of modes than CMB lensing, and ongoing and upcoming surveys (e.g. the Dark Energy Spectroscopic Instrument (DESI; [42–44]), Euclid [45], the Nancy Grace Roman Space Telescope [46], and SPHEREx [47]) are pushing to ever-larger volumes. In [27], using galaxy power spectrum measurements from the completed Baryon Oscillation Spectroscopic Survey (BOSS DR12; [48, 49]), the authors obtained a measurement of the Hubble constant without the sound horizon by using an uninformative prior on the physical baryon density $\omega_{\rm b} \equiv \Omega_{\rm b} h^2$. This method has the benefit of simplicity and leaves the physical size of the sound horizon uncalibrated, but as we explain in section 2, $\omega_{\rm b}$ also contributes to multiple physical effects that constrain H_0, and removing this information is not ideal. In [50], a technique was demonstrated to rescale and marginalize over the sound horizon scale during inference, thus allowing the use of an informative $\omega_{\rm b}$ prior while removing information from the sound horizon scale. Building on this technique, [51] obtained a 3.6% measurement of the Hubble constant by combining BOSS power spectra with *Planck* CMB lensing and SNe Ia from the Pantheon+ dataset.

[1] We note that there is a subtle distinction between the sound horizon distance at photon decoupling ($r_{\rm s}$, which sources features in the CMB), and the sound horizon distance at baryon decoupling ($r_{\rm d}$, which sources baryonic features in the matter power spectrum) [15, 16]. Where the distinction is not important we refer simply to the "sound horizon."

JCAP06(2025)020

In this work, we perform a similar (but blind) measurement to that of [51], using data from the first public data realease of the Dark Energy Spectroscopic Instrument (DESI 2024; [52]). We note that we performed our analysis "blind" in the sense that we only tested our pipeline using mocks before finally running on real data. We combine our result with CMB lensing data from ACT [31, 32] and *Planck* [33–36]. We further increase the precision of our measurement by including additional $\Omega_{\rm m}$ information from two sources: the Alcock-Paczyński (AP) effect [53] observed in the DESI 3D Lyman-α (Lyα) forest [54], and uncalibrated type Ia supernovae. This work represents the most precise measurement of its kind to date, achieving a sub-3% sound horizon-free measurement of H_0. The remainder of this paper is laid out as follows. In section 2 we discuss how each dataset used in this work helps to constrain the Hubble constant without including information from the sound horizon scale, and then in section 3 we describe each specific dataset in detail. In section 4 we describe the steps and components of our analysis pipeline. We present the results of our analysis in section 5, followed by a discussion in section 6. Finally, we conclude in section 7.

2 Theory and methodology

The galaxy power spectrum contains multiple sources of information that contribute to measuring H_0. On one hand there is geometrical information; one form that this takes is in so-called "standard rulers," or features of the power spectrum that correspond to theoretically known distance scales. This includes the sound horizon scale at baryon-photon decoupling $r_{\rm d}$, which determines the structure of the BAO wiggles, as well as the baryonic Jeans suppression scale [55]. Another standard ruler is the matter-radiation equality scale $k_{\rm eq}$, which manifests as the turnover scale of the power spectrum, and also modulates its shape[2] and impacts its amplitude on smaller scales [29]. The observed scale (in angles/redshifts) of a given standard ruler is then a function of both its physical size as well as the distance to the tracer it is measured from, both of which are predicted by a cosmological model. This leads to a measurement of the relevant cosmological parameters (or combinations thereof), where the Hubble constant in particular is inversely proportional to the implied physical distances. Further geometrical information is gained by jointly analyzing tracers at multiple redshifts. Because $k_{\rm eq} \propto \Omega_{\rm m} h$ (when measured in $h\,{\rm Mpc}^{-1}$ units; see equation (2.2)), constraints based on the matter-radiation equality scale $k_{\rm eq}$ display a characteristic degeneracy in the $\Omega_{\rm m} - h$ plane. However, because we observe power spectrum features in angles ($\theta_{\rm eq} \sim \ell_{\rm eq}^{-1} \sim (D_{\rm A}(z)\, k_{\rm eq})^{-1}$) and redshifts ($\Delta z_{\rm eq} \sim H(z)/k_{\rm eq}$) rather than physical distances, this degeneracy direction varies with redshift according to the assumed fiducial cosmological model. The resulting constraints, while largely degenerate for any individual tracer, then intersect at different angles, resulting in a more precise joint constraint (assuming they are consistent and can be combined). A similar phenomenon arises in BAO analyses (see for example figure 2 of [14]).

Somewhat related to geometrical information is the Alcock-Paczyński (AP) effect [53]. When a fiducial cosmology is used to transform galaxy positions from redshift space (R.A., Dec., z) to Cartesian space (x, y, z), any difference between the assumed cosmology and

[2] As discussed in [27], $k_{\rm eq}$ appears non-trivially in the shape of the logarithmic enhancement on scales $k > k_{\rm eq}$.

JCAP06(2025)020

true cosmology will cause clustering features to appear stretched along/across the line of sight. This fictitious distortion is known as the AP effect, and can be related to the true matter density $\Omega_{\rm m}$ (e.g. [54]). Importantly, the AP distortion is independent of absolute distance scales, and thus we can use it to help to break the $\Omega_{\rm m} - H_0$ degeneracy alluded to earlier. Measuring the AP effect requires modelling the full anisotropic contribution to the clustering signal, known as redshift space distortions (RSD), where the latter are also induced by peculiar velocities related to the growth of structure. Because of its dependence on the peculiar velocity field, the RSD measurement can be used to obtain information about the amplitude of the power spectrum, which also has some degeneracy with the Hubble constant (see section 5). Beyond geometric sources, the AP effect, and RSD, note that there is still additional information contained in the shape of the power spectrum. For example, [41] demonstrated a method to derive H_0 using energy density measurements, making use of (among other measurements) the amplitude of the BAO signal from galaxy clustering while marginalizing over the physical sound horizon scale.

Because we want to capture as much information as possible, we choose to analyze the entire shape of power spectrum, rather than any single feature. To do this we use a `Full Modeling` approach (adopting the terminology of [56]), in which we directly generate model power spectrum multipoles from cosmological parameters and fit them to the observed data. This is in contrast to compression-based approaches, in which compressed parameters are fit to the data in a more model-independent way. A ubiquitous example of this is the $\alpha_\parallel$, $\alpha_\perp$ (or $\alpha_{\rm iso}$, $\alpha_{\rm AP}$) parameterization used in BAO analyses (e.g. [12]). Recently, there have been extensions of this approach to full-shape analyses, e.g. `ShapeFit` [57], which uses a template power spectrum to fit for individual effects (RSD, Alcock-Paczyński, etc.) with respect to the fiducial cosmology (see e.g. [28] for a precise sound horizon-independent measurement of H_0 using the ShapeFit approach). While the Full Modeling approach is more computationally expensive, it captures all of the available information without compression (see e.g. [58–60] for comparisons of Full Modeling and compression/template-based techniques).

In ΛCDM the sound horizon at the redshift of baryon-photon decoupling $z_{\rm d}$ (also known as the baryon drag epoch) is given by:

$$\begin{aligned} r_{\rm d} &\equiv \int_{z_d}^{\infty} \frac{c_{\rm s}(z)}{H(z)}\, dz \\ &\approx \frac{55.154 h \exp\left[-72.3\,(\omega_\nu + 0.0006)^2\right]}{\omega_{\rm cb}^{0.25351}\omega_{\rm b}^{0.12807}} \left[h^{-1}{\rm Mpc}\right] \end{aligned} \tag{2.1}$$

[61], where $c_{\rm s}$ is the speed of sound in the photon-baryon plasma prior to decoupling, and $\omega_{\rm cb} \equiv \omega_{\rm cdm} + \omega_{\rm b}$. On the other hand, the matter-radiation equality scale can be calculated as:

$$k_{\rm eq} = \left(2\Omega_{\rm cb} H_0^2 z_{\rm eq}\right)^{1/2} \approx 7.46 \times 10^{-2} \Omega_{\rm cb} h \Theta_{2.7}^{-2} \left[h\,{\rm Mpc}^{-1}\right] \tag{2.2}$$

[16], where $\Theta_{2.7} \equiv T_{\rm CMB}/(2.7\,{\rm K})$. Naturally, the full shape of the power spectrum contains information from both scales, and we would like to remove the sound horizon information from our measurement. In [27], it was shown that this can be accomplished simply by performing a Full Modeling analysis with an uninformative prior on $\omega_{\rm b}$. In this way, the

JCAP06(2025)020

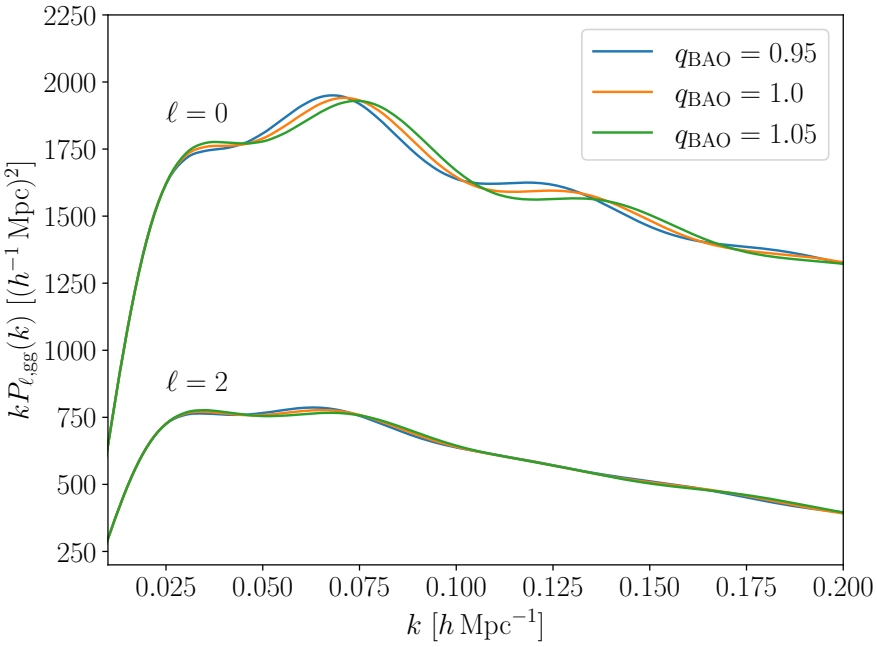

Figure 1. A visual demonstration of the heuristic sound horizon rescaling technique used in this work. Adopting the methodology developed in [50], we rescale the power spectrum wiggles by a free parameter q_{BAO}. Shown above are the monopole ($\ell = 0$) and quadrupole ($\ell = 2$) of the theoretical galaxy power spectrum of DESI LRGs in the redshift range $0.4 < z < 0.6$, for three values of q_{BAO}. $q_{\mathrm{BAO}} = 1.0$ corresponds to the ΛCDM prediction (no rescaling of the sound horizon), whereas $q_{\mathrm{BAO}} = 1.05$ and $q_{\mathrm{BAO}} = 0.95$ have the effect of moving the wiggles forward and backward, respectively.

physical size of the sound horizon remains uncalibrated,[3] and thus cannot be used as a standard ruler in the measurement of H_0. However, this method has the disadvantage of weakening other sources of H_0 information that also depend on the baryon density, e.g. the matter-radiation equality scale, or the critical density of the Universe (in the sense of [41]). An improved method, demonstrated in [50] and subsequently used in [51], heuristically rescales and marginalizes over r_{d} while still allowing the use of an informative prior on ω_{b}. We adopt this approach, which we describe below.

We first split the linear power spectrum into a smooth and wiggly component. To accomplish this, we use a simple version[4] of the method described in appendix D of [62] to obtain the smooth part of the power spectrum, where the wiggly part can then be obtained as the difference between the original power spectrum and the smooth part. We refer the reader to the given reference for details of the method; here we give only a brief summary. The broadband shape of the power spectrum is first divided out using the smooth Eisenstein-Hu formula [16], resulting in an approximation of the wiggles. Then, the gradient of the latter is calculated numerically and extremized. The maxima and minima thus obtained correspond to the nodes of the wiggles; importantly, the smooth part must also pass through these

[3]The authors noted that in principle, r_{d} can be self-calibrated from the combination of the BAO wiggles and the baryonic Jeans suppression scale, but this was not a strong enough prior at the precision of BOSS. In [50] the authors further demonstrated that this effect is not expected to be significant even for a Euclid-like survey.

[4]https://github.com/cosmodesi/cosmoprimo/blob/main/cosmoprimo/bao_filter.py#L472.

JCAP06(2025)020

nodes. Two smooth functions are fit using quadratic splines: one each crossing the nodes that correspond to the gradient maxima or minima, and these curves are finally averaged to give the smooth part of the power spectrum.

Once the smooth and wiggly components have been separated using the above technique, we rescale only the wiggly part by a new parameter $q_{\rm BAO}$ (called $\alpha_{r_{\rm s}}$ in [50]). We then recombine the two components, such that the transformed linear power spectrum can be described as:

$$P_{\rm lin}\left(k, q_{\rm BAO}\right) = P_{\rm lin}^{\rm smooth}\left(k\right) + P_{\rm lin}^{\rm wiggly}\left(q_{\rm BAO} \cdot k\right) \tag{2.3}$$

We can then use this modified linear power spectrum as an input to our full non-linear galaxy clustering model, described in section 4.3. Roughly speaking, the effect of this heuristic transformation is to rescale $r_{\rm d}$ by a factor $q_{\rm BAO}^{-1}$, phenomenologically capturing any modifications to the physics that determines the scale of this feature. In figure 1 we show visually the rescaling of the galaxy power spectrum monopole and quadrupole for three values of $q_{\rm BAO}$. Note that $q_{\rm BAO} = 1.0$ corresponds to ΛCDM (no rescaling), while larger (smaller) values of $q_{\rm BAO}$ shift the BAO wiggles forward (backward). By allowing $q_{\rm BAO}$ to vary freely, the information from the sound horizon scale is marginalized over during inference. We note that several tests were performed in [50] and [51] to demonstrate that the constraints obtained from this procedure are indeed independent of sound horizon information, at least at the precision of DESI and Euclid.

As mentioned earlier, the CMB lensing power spectrum is also sensitive to the matter-radiation equality scale. As discussed in [26], the projection integral relating the lensing power spectrum to the intervening matter power spectrum has the effect of washing out sharp features such as the BAO wiggles. Because of this, CMB lensing is not sensitive to the sound horizon scale,[5] but rather to the broadband shape of the matter power spectrum, which is modulated by the matter-radiation equality scale as noted above. Thus CMB lensing constrains H_0 similarly to above, albeit with a distinct degeneracy direction in the $\Omega_{\rm m} - H_0$ plane, helping to improve the joint constraint.

Clearly, the $\Omega_{\rm m} - H_0$ degeneracy can be broken further by including additional information on $\Omega_{\rm m}$. In this work we consider two additional sources of $\Omega_{\rm m}$ information. The first of these is type Ia supernovae (SNe Ia). SNe Ia are standardizable candles that trace the expansion history of the Universe. When the local distance ladder [2, 63] is used to calibrate the absolute magnitudes of SNe Ia, their observed brightnesses imply physical distances, and they can be used to measure H_0. When left uncalibrated they no longer provide absolute distance information, but still probe the expansion history. In a flat universe and for a fixed dark energy equation of state, this primarily provides information on $\Omega_{\rm m}$. The second source of $\Omega_{\rm m}$ information we include in our measurement is the AP effect observed in the full-shape 3D Lyman-α forest power spectrum [54, 64, 65]. As mentioned above, information from the AP effect is also included in galaxy clustering, however the effect is stronger for the Lyα forest as it is more sensitive to small-scale structures [64]. The Lyα forest [66, 67] can be seen in the spectra of distant quasars, and traces the density of the intervening

[5] In [26], the authors additionally verify that no significant information is sourced from the baryonic Jeans suppression scale.

JCAP06(2025)020

neutral hydrogen. As light travels toward us from a quasar and becomes redshifted by the expansion of space, it can be absorbed by neutral hydrogen (in this case as Lyα photons). Thus we observe a "forest" of absorption lines in the quasar spectrum, blueward of the quasar's rest-frame Lyα wavelength. By considering the emitted wavelength of the quasar light and the strength of its absorption, the structure of the intervening neutral hydrogen can be inferred. The AP distortion observed in the Lyα forest power spectrum then provides information on $\Omega_{\rm m}$, as discussed previously.

3 Data

Here we describe each specific dataset used in this work.

3.1 Galaxies and the Lyman-α forest

The Dark Energy Spectroscopic Instrument (DESI) is a multi-object spectrographic survey performed using ∼5,000 robotically positioned fibers and operating on the Mayall 4-meter telescope at Kitt Peak National Observatory [43, 68–70]. DESI is currently conducting a five-year survey that will cover roughly 14,000 deg^2 of the sky and obtain the spectra of more than 40 million galaxies and quasars [42]. The main science goal of the survey is to probe the nature of dark energy via the most precise measurement of the expansion history of the Universe to date [71]. The spectroscopic data reduction pipeline used for DESI is described in [72], while the survey operations and observation plan are detailed in [73]. DESI target selection is based on imaging data from the public DESI Legacy Imaging Surveys [74]. The DESI scientific program was validated in [44], accompanied by an early data release [75].

The first-year data release of the DESI survey (DESI 2024; [52]) contains the positions and spectra of over 5.7 million unique objects, which are classified among several tracers in multiple redshift bins. Accompanying the DESI 2024 data release are several science Key Papers: two-point clustering measurements and validation [76], measurements of the BAO feature in galaxies and quasars [12] and the Lyman-α (Lyα) forest [13], and the full-shape study of galaxies and quasars [77]. Cosmological interpretations were given for the BAO measurements [14] and the full-shape analysis [56]. In this work we jointly analyze the full-shape clustering of a total of six unique tracer/redshift combinations in DESI 2024: the low-redshift bright galaxy sample (BGS) at redshift range $0.1 < z < 0.4$, luminous red galaxies (LRGs) in three redshift bins ($0.4 < z < 0.6$, $0.6 < z < 0.8$, and $0.8 < z < 1.1$), emission line galaxies (ELGs) in the redshift range $1.1 < z < 1.6$, and quasars (quasi-stellar objects or QSOs) in the redshift range $0.8 < z < 2.1$, together comprising a total of 4.7 million galaxies. Additionally, we make use of measurements of the Lyα forest, as observed in the spectra of distant DESI quasars. In particular, we use the measurement by [54] of the Alcock-Paczyński effect observed in the 3D power spectrum of the DESI Lyα forest.

3.2 CMB lensing

We use a combination of CMB lensing data from the *Planck* [3] and ACT [8, 78] surveys. Specifically, we use the *Planck* NPIPE PR4 lensing reconstruction [36], which covers ∼27,600

JCAP06(2025)020

deg^2 of the sky, and the ACT DR6 lensing reconstruction [8, 78], covering 9,400 deg^2. We make use of the publicly available[6] *Planck*+ACT CMB-marginalized lensing-only likelihood.

3.3 Type Ia supernovae

As in [14] and [56], we combine our results with three separate uncalibrated supernova datasets. Because uncalibrated SNe Ia primarily constrain $\Omega_{\rm m}$ (as was noted in section 2), we choose to extract $\Omega_{\rm m}$ priors from each dataset rather than working with the full posteriors, which would provide little additional information. We perform the combination with each supernova dataset individually, without favoring any one over the other. These datasets are the Dark Energy Survey Year 5 supernova analysis (DESY5; [79]), Pantheon+ [80], and Union3 [81]. We very briefly describe each dataset, referring the reader to the relevant references for further information. DESY5 represents the largest and most homogeneous single sample of high-redshift supernovae to date; it combines novel observations of 1,635 photometrically classified SNe Ia (spanning $0.1 < z < 1.3$) with existing observations of 194 low-redshift ($0.025 < z < 0.1$) SNe Ia, the latter of which are also shared by Pantheon+. The Pantheon+ dataset itself is a compilation of data from many surveys; it contains four separate high-redshift samples ($z > 1.0$), three mid-redshift samples ($0.1 < z < 1.0$), and 11 different low-redshift samples ($z < 0.1$), for a total of 1,550 spectroscopically confirmed SNe Ia. Union3 consists of 2,087 SNe Ia, sharing 1,363 with Pantheon+, and additionally makes use of a Bayesian Hierarchical Modeling approach in its likelihood analysis.

4 Likelihood and analysis

Here we describe the settings and techniques used in our analysis. The entire analysis pipeline is built into the code `desilike`.[7] Throughout this work we assume a cosmology with $\tau_{\rm reio} = 0.0544$, $N_{\rm eff} = 3.046$, and three degenerate species of massive neutrinos as in [3].

4.1 Data vector

We filter the galaxy power spectrum multipoles measured in DESI 2024 for each tracer to wavenumber k in the range $[0.02, 0.20]\ h\,{\rm Mpc}^{-1}$ for $\ell = 0, 2$, in steps ${\rm d}k = 0.005\,h\,{\rm Mpc}^{-1}$. This is consistent with the analyses of [56, 77], however we note that the k-range of our data vector does not include the expected turnover scale of the power spectrum, $k_{\rm eq} \sim 0.015\,h\,{\rm Mpc}^{-1}$. As remarked in section 2, the matter-radiation equality scale not only sets the turnover scale of the power spectrum, but also appears non-trivially in its broadband shape. In fact, [29] showed that for data from BOSS, the scales $k > k_{\rm eq}$ are dominant over the position of the turnover scale in constraining H_0 without the sound horizon. We expect this also to be the case for the first DESI data release, but this may change in the future as the peak of the power spectrum becomes better resolved.

All additional processing of the data, including truncation of small angular scales [82], "rotation" of the data vector to compactify the window matrix in k-space [82], and corrections for the radial integral constraint (RIC) [83] and angular integral constraint (AIC) [76], directly

[6] https://github.com/ACTCollaboration/act_dr6_lenslike. We enforced the following settings for our analysis: `variant = actplanck_baseline` and `lens_only = true`.

[7] https://desilike.readthedocs.io.

JCAP06(2025)020

follows the methodology described in [76]. The latter two effects (the RIC and AIC) are particularly important to account for in this analysis, as they lead to the damping of power on large radial and angular scales, respectively. In summary, the RIC arises because the redshift distribution of randoms exactly matches that of the data (by design), while the AIC is caused by the use of imaging systematic weights that are obtained by regressing the galaxy density on several maps that encode various imaging properties. Both effects are individually corrected by comparing the mean power spectra of mocks that do/do not contain the particular effect, and fitting a polynomial to capture the difference in power.

4.2 Covariance matrix

We use a covariance matrix that is a sum of both a statistical and systematic component. The statistical part of the covariance matrix is described in detail in [84], whereas the systematic contributions are given in [77], with the detailed methodology of their combination shown in appendix D of the latter. The statistical part of covariance matrix was calculated using 1,000 EZmocks (effective Zel'dovich approximation mocks, [85]), which are faster to create than full N-body simulations, while still accurately capturing the DESI 2024 clustering statistics. As discussed in [77], any systematic effect that leads to a parameter-level bias of at least 0.2σ (in units of the DESI 2024 error) is included in the systematic component of the covariance matrix. These systematic contributions include imaging effects, fiber assignment, and halo occupation distribution (HOD)-dependent systematics. Once added in quadrature, these effects contribute a systematic uncertainty of $\sim 0.46\sigma$ in units of the DESI 2024 error, which is much smaller than the sound horizon-marginalized error level of this work.

4.3 Power spectrum model

To calculate the theoretical galaxy power spectrum, we use the publicly available code `velocileptors`[8] [86, 87], which is based on the effective field theory of large-scale structure (EFT of LSS). We use the Lagrangian perturbation theory (LPT) implementation up to third order, fixing the third-order bias parameter b_3 to zero similarly to [56, 77]. We adopt a physically motivated reparameterization of the EFT biases, counterterms, and stochastic terms, which is outlined in [77]. By using this parameterization, physically interpretable priors can be enforced on these parameters, as discussed in section 4.4.

4.4 Priors

Our prior choices largely follow [56, 77], and we summarize them below while noting any differences. The baseline Bayesian priors used in this work (that is, for constraints from the DESI data alone) are shown in table 1. In summary, we sample the cosmological parameters H_0, Ω_m, ω_b, $\ln(10^{10} A_\mathrm{s})$, n_s, and q_BAO, as well as bias parameters in the basis $(1+b_1)\,\sigma_8$, $b_2\sigma_8^2$, $b_s\sigma_8^2$ (chosen to reduce projection effects, described below), while enforcing a maximization procedure on the counterterms $\alpha_{[0,2,4]}$ and stochastic parameters $\mathrm{SN}_{[0,2,4]}$ that efficiently approximates a Jeffreys prior [88, 89]. We note that we sample the parameter Ω_m instead of ω_cdm as in [56, 77], and we also allow the nuisance parameters α_4 and SN_4 to vary rather than fixing them to zero (the latter corresponds to an older analysis configuration and will

[8] https://github.com/sfschen/velocileptors.

JCAP06(2025)020

cause our parameter errors to be slightly more conservative). Additionally, use of the Jeffreys prior is unique to this work, and we discuss it in depth at the end of this section. We fix the sum of the neutrino masses, $\sum m_\nu$, to 0.06 eV.[9] We include two external priors: a Big Bang Nucleosynthesis (BBN) prior on ω_b [91], and a wide Gaussian prior on n_s with standard deviation 0.042, corresponding to 10× the width of the posterior reported by the *Planck* collaboration using both the primary CMB fluctuations and their gravitational lensing by large-scale structure (TT,TE,EE+lowE+lensing) [3]. When combining our results with CMB lensing, we enforce the narrower n_s prior employed in the *Planck* lensing-only analysis: $n_\mathrm{s} \sim \mathcal{N}\left(0.96, 0.02^2\right)$ [35]. We enforce Gaussian priors on the EFT counterterms $\alpha_{[0,2,4]}$ such that the 1σ correction to the power spectrum at $k_\mathrm{max} = 0.2\,h\,\mathrm{Mpc}^{-1}$ is at most 50% of the total signal; this translates to a $\mathcal{N}\left(0, 12.5^2\right)$ prior [77]. For the stochastic terms, we enforce a Gaussian prior $\mathcal{N}\left(0, 2^2\right) \times 1/\bar{n}_\mathrm{g}$ on the monopole term SN_0, corresponding to a width of 2× the Poissonian shot noise, and $\mathcal{N}\left(0, 5^2\right) \times f_\mathrm{sat}\sigma^2_{1\,\mathrm{eff}}/\bar{n}$ for SN_2, corresponding to a width of 5× the characteristic velocity dispersion, where f_sat is the expected satellite galaxy fraction and $\sigma^2_{1\,\mathrm{eff}}$ is the velocity dispersion of these galaxies. SN_4 uses a prior with the same width as SN_2, but with an additional factor of $\sigma^2_{1\,\mathrm{eff}}$.

As mentioned above, we differ from [56, 77] in applying an approximate Jeffreys prior [88] to a subset of the parameters comprised by the counterterms and stochastic terms. Bayesian inference using EFT models, which have a very high-dimensional space of nuisance parameters, is generally prone to parameter biases due to what are known as prior weight effects and prior volume effects, collectively called "projection effects" [92, 93]. The Jeffreys prior, by construction, minimizes sensitivity to the choice of parameterization and therefore also minimizes projection effects. In [56] it is shown that for full-shape analysis of the DESI 2024 data, projection effects can become pronounced when opening up the parameter space beyond standard ΛCDM (which we are doing through the addition of the q_BAO parameter). Indeed, when analyzing mock DESI data alone without a Jeffreys prior, we observe H_0 offsets at the $\sim 2\sigma$ level; these offsets are corrected almost entirely after enforcing a Jeffreys prior. While the addition of external datasets can help to mitigate biases due to projection effects [56, 89], we conservatively choose to apply the Jeffreys prior to further reduce these effects. We efficiently accomplish this using the technique of [89], who showed that the profile likelihood is a good approximation for a nuisance parameter-marginalized posterior in the presence of a Jeffreys prior. In other words, we simply fix our nuisance parameters (counterterms and stochastic terms) to their best-fit (maximum posterior) values at each point in cosmological+bias parameter space.

4.5 Emulator

A single evaluation of the full EFT theory can take several seconds, which can be prohibitively time-consuming for a single Markov chain Monte Carlo run (MCMC; see [94] and references therein), let alone the many runs needed for testing. We therefore train an emulator to quickly

[9] In [51], it is noted that $\sum m_\nu$ has some degeneracy with H_0, especially in the CMB lensing likelihood. However, they obtained nearly identical constraints when fixing this parameter compared to enforcing their fiducial prior $\sum m_\nu < 0.26\,\mathrm{eV}$, i.e. the 2σ constraint from the *Planck* primary CMB [3]. While we consider their fiducial prior sufficiently conservative, we note that the authors observed degraded constraints when using a prior several times wider, e.g. from the ground-based KATRIN experiment [90].

JCAP06(2025)020

Parameter	Prior	Notes
H_0	Unif $[20, 100]$	$[\mathrm{km\,s^{-1}\,Mpc^{-1}}]$
Ω_m	Unif $[0.01, 1.0]$	
ω_b	$\mathcal{N}\left(0.02218, 0.00055^2\right)$	BBN [91]
$\ln\left(10^{10} A_\mathrm{s}\right)$	Unif $[1.61, 3.91]$	
n_s	$\mathcal{N}\left(0.9649, 0.042^2\right)$	10× *Planck* [3]
q_BAO	Unif $[0.9, 1.1]$	
$(1 + b_1)\,\sigma_8$	Unif $[0.0, 3.0]$	
$b_2\sigma_8^2$, $b_s\sigma_8^2$	$\mathcal{N}\left(0, 5^2\right)$	
α_0, α_2, α_4	$\mathcal{N}\left(0, 12.5^2\right)$	+Approx. Jeffreys prior[a]
SN_0	$\mathcal{N}\left(0, 2^2\right) \times 1/\bar{n}_\mathrm{g}$	+Approx. Jeffreys prior[a]
SN_2	$\mathcal{N}\left(0, 5^2\right) \times f_\mathrm{sat}\sigma^2_{1\,\mathrm{eff}}/\bar{n}_\mathrm{g}$	+Approx. Jeffreys prior[a]
SN_4	$\mathcal{N}\left(0, 5^2\right) \times f_\mathrm{sat}\sigma^4_{1\,\mathrm{eff}}/\bar{n}_\mathrm{g}$	+Approx. Jeffreys prior[a]

[a] Jeffreys prior [88] applied in addition to the listed Gaussian prior. In practice, we use an approximation to the Jeffreys prior demonstrated in [89] (see section 4.4).

Table 1. Priors used in this work for constraints from the DESI data alone. The physically motivated nuisance parameterization used here is described in detail in [77] and [58]. The prior width of the term SN_0 is multiplied by the Poissonian shot noise $1/\bar{n}_\mathrm{g}$, whereas the prior width for the term SN_2 is multiplied by the expected satellite galaxy fraction times the mean satellite velocity dispersion times the Poissonian shot noise, corresponding to the characteristic velocity dispersion [58], and so on for SN_4.

produce approximate theoretical power spectrum multipoles at any given point in cosmological parameter space. We train a 4th-order Taylor series emulator for each tracer, a functionality that is built into the `desilike` code.[10] `desilike` separates the cosmology- and nuisance-dependent parts of the perturbation theory integrals (with the former consuming the bulk of the computation time), so that we only need to Taylor expand in the cosmological parameters.

4.6 Sampling

We run MCMC inference using the `desilike` implementation of the No-U-Turn sampler (NUTS; [95]) on the Perlmutter computing cluster at the National Energy Research Scientific Computing Center (NERSC). We continue sampling until the maximum-eigenvalue Gelman-Rubin statistic [96] satisfies $R - 1 < 0.03$. Because the coverged MCMC chains were generated using the emulated EFT theory, after sampling we chose to recover the true posterior distribution via importance sampling. That is, we weight each point in the chain by the ratio of the true posterior probability to emulated posterior probability.[11] We note

[10] https://desilike.readthedocs.io/en/latest/api/emulators.html#module-desilike.emulators.taylor.

[11] We note that when importance sampling with the true theory, we use the same maximization technique described in section 4.4 for the counterterms and stochastic terms. That is, at a given point in cosmological+bias parameter space, we use the best-fit counterterms and stochastic terms according to the true posterior.

JCAP06(2025)020

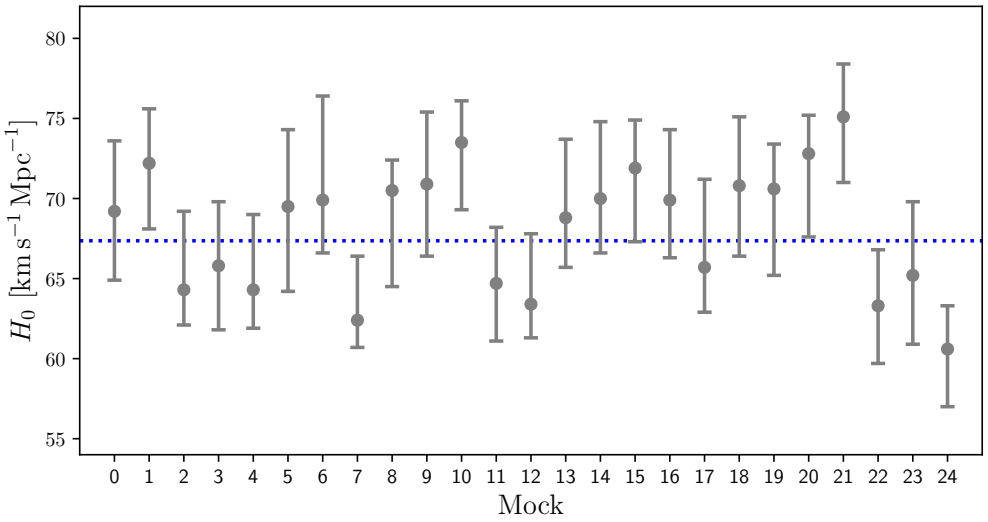

Figure 2. 68% credible-interval constraints on the parameter H_0, for all 25 AbacusSummit mocks used for the testing of our analysis pipeline. The blue dotted line shows the true underlying H_0 value of the mocks. 18 of the 25 credible intervals (72%) capture the true H_0 value.

that after unblinding our analysis, in order to obtain very well-sampled chains for the final combination with several external datasets, we resumed sampling until obtaining an effective sample size (ESS) of 40,000, defined as the total number of MCMC iterations divided by the integrated correlation length of the chains. These are the chains that were used to derive the results presented in this work.

4.7 Validation on mocks and unblinding

We chose to perform our analysis "blind" in order to avoid introducing human bias into the results. Rather than blinding via a random transformation of the real data (as was done in [77]), by "blind" we mean that we only tested our analysis settings and pipeline using mocks, before finally deciding to run and view our results using the real data. For our mock testing, we used 25 mock data vectors obtained from AbacusSummit [97, 98] N-body mocks, which are based on halo occupation distribution (HOD) models calibrated to match the clustering of the DESI early data release [75]. The specific mocks we used for testing are described in [99–101]. We used the same covariance matrix described in section 4.2.

Before running our analysis on real data, we ensured that the following criteria were satisfied. First, we confirmed that among the 25 mock measurements, roughly 68% of our 1σ H_0 constraints captured the fiducial value used in the mocks. The results of this test using mock DESI data alone are shown in figure 2, which shows that 18 of the 25 constraints, or 72%, capture the true H_0 value used in the mocks. Additionally, we observed no significant biases in the parameter constraints when considering two different mock fiber assignment strategies (Fast Fiber Assign [102] and altMTL [103]). As a final check before unblinding our results, we ran our analysis pipeline on the real DESI data, and importance sampled the emulated chains using the true theory as described in section 4.6. We confirmed (only looking at differences in parameter values) that the mean H_0 values obtained from the emulated and

JCAP06(2025)020

Dataset(s)	H_0 [$\mathrm{km\,s^{-1}\,Mpc^{-1}}$]
DESI galaxy clustering only	71.2 ± 4.1
DESI + CMB lensing	$70.1^{+2.7}_{-3.3}$
DESI + CMB lensing + $\Omega_\mathrm{m}^\mathrm{Ly\alpha AP}$	$69.6^{+2.4}_{-2.6}$
DESI + CMB lensing + $\Omega_\mathrm{m}^\mathrm{DESY5}$ (+ $\Omega_\mathrm{m}^\mathrm{Ly\alpha AP}$)	$66.1^{+1.8}_{-2.0}$ $\left(66.7^{+1.7}_{-1.9}\right)$
DESI + CMB lensing + $\Omega_\mathrm{m}^\mathrm{Pantheon+}$ (+ $\Omega_\mathrm{m}^\mathrm{Ly\alpha AP}$)	$67.6^{+1.9}_{-2.2}$ $\left(67.9^{+1.9}_{-2.1}\right)$
DESI + CMB lensing + $\Omega_\mathrm{m}^\mathrm{Union3}$ (+ $\Omega_\mathrm{m}^\mathrm{Ly\alpha AP}$)	$67.3^{+2.1}_{-2.4}$ $\left(67.8^{+2.0}_{-2.2}\right)$

Table 2. H_0 constraints obtained in this work. Limits shown are 68% credible intervals.

importance-sampled chains differed by less than 0.3σ. After satisfying this final criterion, we unblinded our results and combined with external datasets as described in section 4.8. We note that our fiducial datasets for this work, i.e. those chosen before unblinding, were: 1) DESI galaxy clustering; 2) *Planck*+ACT CMB lensing; and 3) Ω_m information from each of the DESY5/Pantheon+/Union3 SN-Ia datasets. After unblinding, we decided to further combine our result with Ω_m information from the DESI Lyα forest as described in section 2. Both sets of results are presented in section 5. Additionally, we note that our initial run on real data did not include the clustering of the BGS sample; however, this negligibly affected our main results.

4.8 Combination with external datasets

In this paper we combine the base DESI clustering-only analysis with external data at the likelihood level by reweighting our MCMC chains. In the case of CMB lensing, we perform importance sampling using the *Planck*+ACT likelihood described in section 3. We note that the combination with CMB lensing at the likelihood level is permissible because the covariance between the projected statistics and the multipoles is negligible [104]. Meanwhile for DESY5 and Pantheon+, we note that the constraints on Ω_m are Gaussian, leading to a simple analytic re-weighting. However, we find that the Union3 and Lyα constraint on Ω_m is not Gaussian, so in these cases we use `CombineHarvesterFlow`[12] [105] to find the joint constraints.

5 Results

The results of this work are summarized in table 2. In figure 3 we present our constraints on the parameters $\{H_0,\ \Omega_\mathrm{m},\ \ln(10^{10}A_\mathrm{s}),\ n_\mathrm{s},\ q_\mathrm{BAO}\}$ using the DESI galaxy clustering data alone (BGS + LRGs + ELGs + QSOs), as well as when combining with *Planck*+ACT CMB lensing and Ω_m information from the DESI Lyα forest ($\Omega_\mathrm{m}^\mathrm{Ly\alpha AP}$). We first note the high quality of the constraints afforded by the DESI data alone, especially considering that we have only analyzed data from the first DESI data release, which corresponds to the first of five total years of observations. In particular, the DESI clustering-only sound horizon-marginalized H_0 constraint, $71.2 \pm 4.1\,\mathrm{km\,s^{-1}\,Mpc^{-1}}$, is already more precise than the analogous constraints

[12] https://github.com/pltaylor16/CombineHarvesterFlow.

JCAP06(2025)020

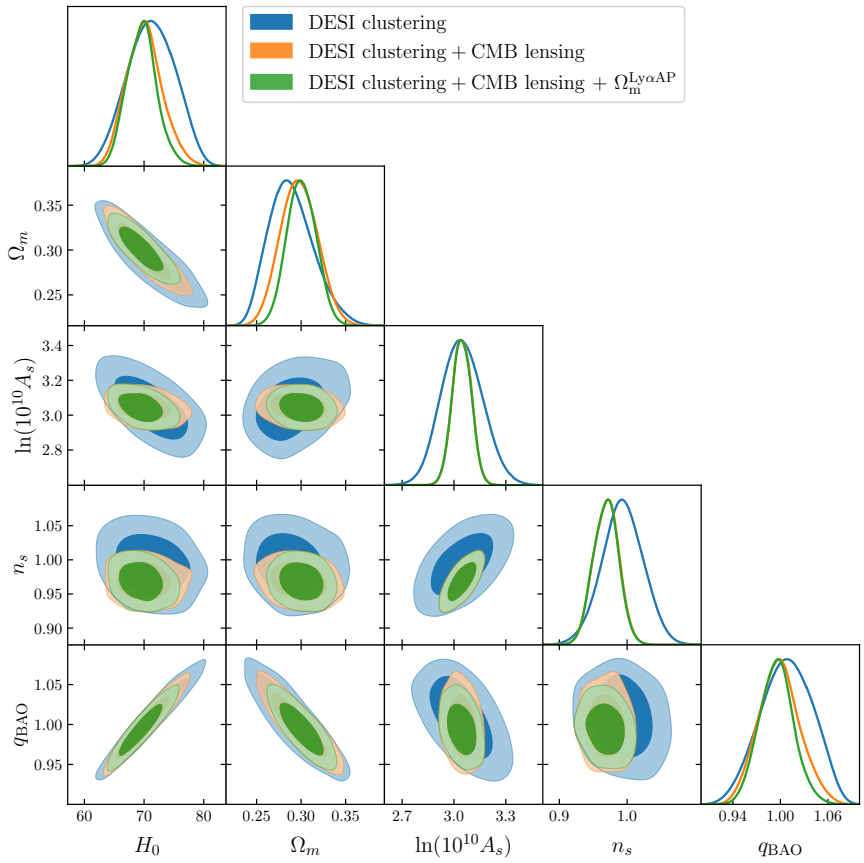

Figure 3. Cosmological parameter constraints from: 1) DESI galaxy clustering only (BGS + LRG + ELG + QSO); 2) DESI clustering + CMB lensing; and 3) DESI clustering + CMB lensing + $\Omega_{\rm m}^{\rm Ly\alpha AP}$. CMB lensing refers to the *Planck*+ACT lensing-only likelihood described in section 3. We note that Lyα was added after unblinding, as discussed in section 4.7.

obtained from BOSS DR12 in [50] and [51]. As discussed in section 2, the six DESI tracers, while individually carrying $k_{\rm eq}$-characteristic degeneracies in the $\Omega_{\rm m} - H_0$ plane, each intersect to create a more precise joint constraint. The addition of CMB lensing primarily helps to improve the H_0 constraint by intersecting the DESI contour at a slightly steeper angle in the $\Omega_{\rm m} - H_0$ plane. To a lesser extent, CMB lensing additionally improves the H_0 measurement by better constraining the amplitude $A_{\rm s}$ of the primordial power spectrum, which also displays some degeneracy with the Hubble constant. With the addition of $\Omega_{\rm m}$ information from the DESI Lyα forest, we obtain our tightest constraints independent of supernovae (DESI clustering + CMB lensing + $\Omega_{\rm m}^{\rm Ly\alpha AP}$): $H_0 = 69.6^{+2.4}_{-2.6}\,{\rm km\,s^{-1}\,Mpc^{-1}}$. We finally note that even when allowing the sound horizon rescaling parameter $q_{\rm BAO}$ to vary freely with an uninformative prior, our data broadly seem to prefer values near the ΛCDM prediction of $q_{\rm BAO} = 1.0$. This is also the case when combining with CMB lensing and $\Omega_{\rm m}^{\rm Ly\alpha AP}$; the full combination of these datasets gives the constraint $q_{\rm BAO} = 0.995^{+0.021}_{-0.022}$.

In figure 4 we show our full constraints on H_0, $\Omega_{\rm m}$, and $q_{\rm BAO}$ using all datasets listed in section 3. On the left we show the three dataset combinations that were chosen before unblinding: DESI galaxy clustering + CMB lensing + $\Omega_{\rm m}^{\rm DESY5}/\Omega_{\rm m}^{\rm Pantheon+}/\Omega_{\rm m}^{\rm Union3}$. On the

JCAP06(2025)020

right we show our tightest constraints, in which we additionally include $\Omega_{\rm m}$ information from DESI Lyα, again noting that this was decided after unblinding (as discussed in section 4.7). Our tightest H_0 constraints obtained in this work are:

$$H_0 = \begin{cases} 66.7^{+1.7}_{-1.9}\ \mathrm{km\,s^{-1}\,Mpc^{-1}} & (\text{DESI + CMB lensing + } \Omega_{\rm m}^{\rm Ly\alpha AP} + \Omega_{\rm m}^{\rm DESY5}) \\ 67.9^{+1.9}_{-2.1}\ \mathrm{km\,s^{-1}\,Mpc^{-1}} & (\text{DESI + CMB lensing + } \Omega_{\rm m}^{\rm Ly\alpha AP} + \Omega_{\rm m}^{\rm Pantheon+}) \\ 67.8^{+2.0}_{-2.2}\ \mathrm{km\,s^{-1}\,Mpc^{-1}} & (\text{DESI + CMB lensing + } \Omega_{\rm m}^{\rm Ly\alpha AP} + \Omega_{\rm m}^{\rm Union3}) \end{cases}$$

This translates to a $\sim$2.9% average constraint, which as far as the authors are aware is the most precise sound horizon-free H_0 measurement to date using a Full Modeling approach.[13] We can interpret our combined constraints on the parameter $q_{\rm BAO}$ as a test of whether the full dataset is consistent with ΛCDM, in the context of sound horizon-modifying new physics. Because our marginalized posteriors are asymmetric, we adopt the non-Gaussian tension estimation technique of [106]. We find that our full joint constraints are consistent with ΛCDM ($q_{\rm BAO} = 1.0$) at up to 1.8σ when including Lyα, or 2.0σ without Lyα. We note that we observe a slight preference for $q_{\rm BAO} < 1.0$, which is driven by the larger $\Omega_{\rm m}$ preferred by the SN Ia datasets relative to DESI. Loosely speaking, this preferentially selects one side of the $\Omega_{\rm m} - H_0$ contour in figure 3, requiring a decrease in $q_{\rm BAO}$ (i.e. an increase in $r_{\rm d}$) to compensate the smaller implied H_0. Future DESI data releases will help to determine whether or not this is simply a statistical fluctuation; it will be particularly important to investigate such deviations in the context of the recent results on dynamical dark energy in DESI DR1 [14, 56].

Finally, we note that because the measurements in this work depend on the broadband shape of the power spectrum, special attention is warranted to determine our sensitivity to large-scale systematics. In appendix A, we demonstrate the robustness of our constraints to several potential sources of such systematic effects.

6 Discussion

In figure 5 we show how the measurements from this work fit into the current landscape of H_0 measurements. We note two interesting observations. First is that even without using information from the sound horizon scale, our tightest H_0 measurements are still in 2.9σ, 2.3σ, or 2.2σ tension with SH0ES, when combining with DESY5, Pantheon+, and Union3 respectively (again, using the non-Gaussian tension estimation technique of [106]). Without including Lyα (our fiducial data choice made before unblinding), these tensions are 3.0σ, 2.3σ, and 2.3σ. Second, our measurement is consistent with other early-time measurements that fully or mostly rely on the sound horizon scale. This would indicate that our measurement is consistent with ΛCDM, and in particular we do not find evidence for new early-Universe physics. We do note, however, that in section 5 we found that the dataset combination (DESI clustering + CMB lensing + $\Omega_{\rm m}^{\rm DESY5}$) reaches a 2.0σ deviation from the ΛCDM prediction of $q_{\rm BAO} = 1.0$, and it will be interesting to see how this changes with the coming three-year and five-year data releases of DESI.

[13] We note that [28] obtained a similarly precise constraint using ShapeFit and data from BOSS DR12; their template-based approach and other differences in their analysis pipeline (in particular their inclusion of "uncalibrated, unnormalized" BAO information, which we plan to investigate in future work) make a direct comparison difficult.

JCAP06(2025)020

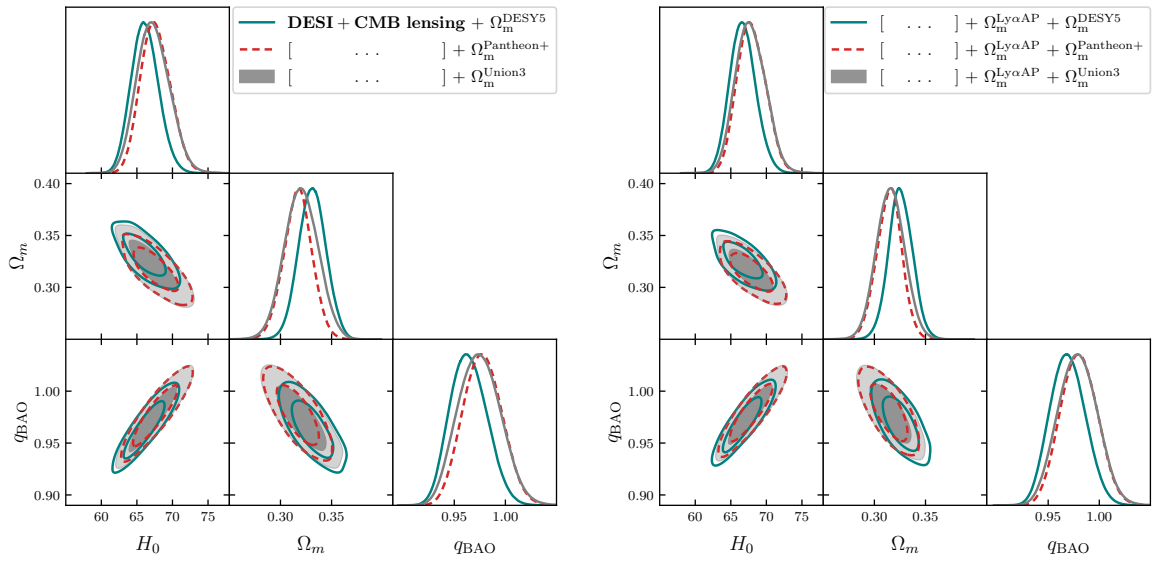

Figure 4. Constraints obtained in this work on the parameters H_0, Ω_m, and q_{BAO}. **Left:** Constraints from DESI galaxy clustering + CMB lensing + Ω_m information from each of the DESY5, Pantheon+, and Union3 supernova datasets. **Right:** Same as left, with the addition of Ω_m information from the DESI Lyα forest, as desribed in section 2. We note that Lyα was added after unblinding. CMB lensing refers to the *Planck*+ACT lensing-only likelihood described in section 3.

In [50], the authors performed a similar analysis for a simulated Euclid-like survey in an early dark energy (EDE) universe. Two EDE models were considered; the best-fit EDE model from *Planck* + SH0ES data ([109]; weaker EDE), and the EDE model favored by ACT ([110]; stronger EDE). They then measured H_0 both with and without sound horizon information (assuming a ΛCDM fiducial cosmology), finding that EDE generally shifts the sound horizon H_0 measurement toward higher values relative to the sound horizon-free measurement, which is expected due to the reduction of the physical sound horizon scale. The consistency we observe in this work between various early-time H_0 measurements, regardless of whether they rely on the sound horizon scale or are independent of it, begins to put pressure on more extreme beyond-ΛCDM models such as ACT-favored EDE.[14] However, we cannot rule out the possibility of less extreme models of new physics (such as *Planck* EDE). The volume probed by galaxy surveys will increase rapidly in the coming years; as more data is collected and the precision of sound horizon-free H_0 measurements improves, even stronger constraints will be placed on such models of new early-Universe physics.

7 Conclusions

In light of the Hubble tension, there is significant interest in measuring the Hubble constant H_0 using independent techniques. We have performed a precise measurement of H_0 without relying on information from the sound horizon scale, using data from the first data release of the DESI survey. In section 2 we demonstrated our methodology for removing the sound

[14] We note that dedicated tests of specific models will be needed to draw rigorous conclusions about their viability.

JCAP06(2025)020

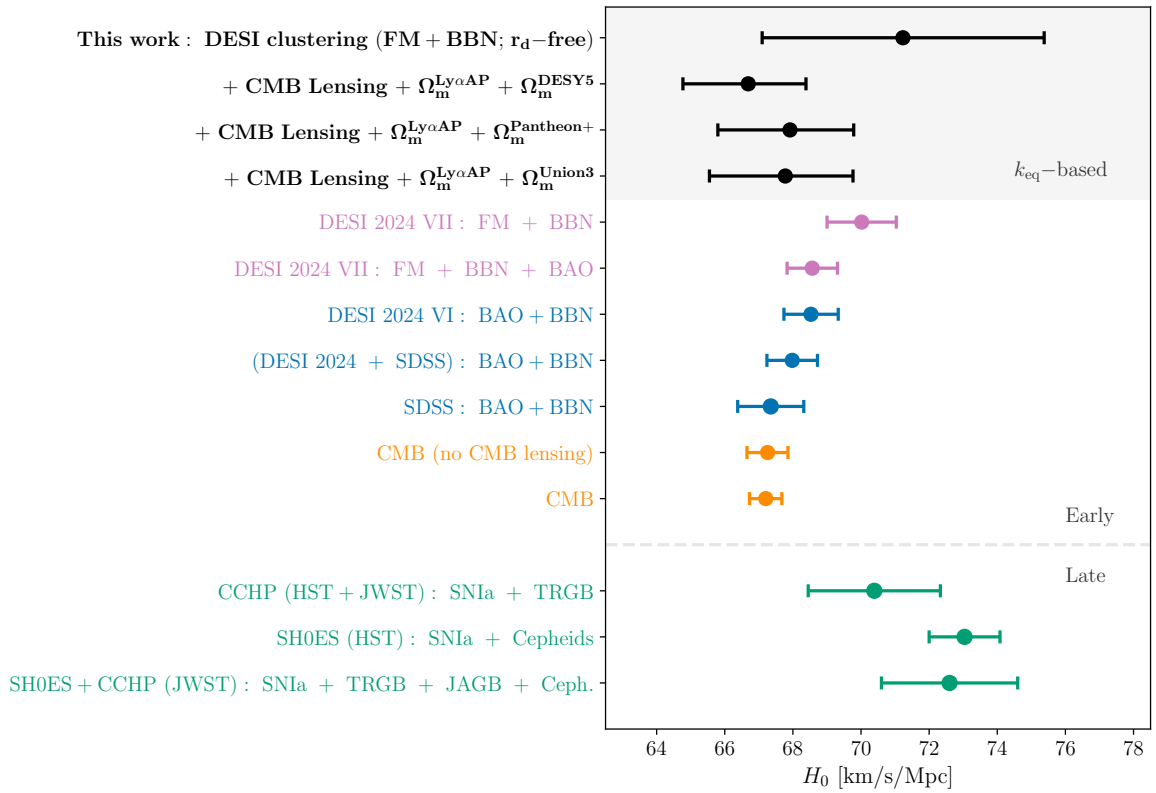

Figure 5. 68% credible interval constraints from various measurements of the Hubble constant. The black whiskers with bolded labels show constraints obtained in this work. We show our H_0 measurement from DESI galaxy clustering alone (BGS + LRG + ELG + QSO), as well as when combined with *Planck*+ACT CMB lensing and Ω_m information from the DESI Lyα forest and each supernova dataset as discussed in section 5. The pink whiskers show constraints from the DESI 2024 full-shape analysis [56], while the blue whiskers show constraints from the DESI 2024 [14] and/or the Sloan Digital Sky Survey (SDSS; [107]) BAO analyses. CMB H_0 measurements from the combination of *Planck* and ACT data are shown in orange. Finally, the green whiskers at the bottom show local distance ladder H_0 constraints from the Chicago-Carnegie Hubble Program (CCHP; [63]) (at the time of writing, in [63] the CCHP team quotes their HST+JWST TRGB-calibrated H_0 measurement as their main result.) using data from the Hubble Space Telescope (HST) and the James Webb Space Telescope (JWST), the SH0ES [2] team using data from HST, as well as combined constraints from the largest combination of both subsamples available in JWST [108]. JAGB stands for the J-region Asymptotic Giant Branch method, and TRGB stands for the Tip of the Red Giant Branch calibration method (see the relevant references for further information).

horizon information from our measurement, rescaling and marginalizing over the sound horizon distance using the technique developed in [50]. By jointly analyzing the full-shape clustering of DESI LRGs, ELGs, quasars, and the bright galaxy sample in six redshift bins, we have obtained constraints that already surpass those from the completed BOSS survey (e.g. [50] and [51]). When further combining with CMB lensing, uncalibrated type Ia supernovae, and Alcock-Paczyński information from the DESI Lyα forest, we have obtained a sub-3% constraint on H_0, the most precise sound horizon-free measurement from LSS to date using a Full Modeling approach.

JCAP06(2025)020

The complete results from this work were shown in section 5. Using the full joint dataset including DESI clustering + CMB lensing + $\Omega_{\rm m}^{\rm SN\,Ia}$ + $\Omega_{\rm m}^{{\rm Ly}\alpha{\rm AP}}$, our tightest H_0 constraints are $66.7^{+1.7}_{-1.9}$, $67.9^{+1.9}_{-2.1}$, and $67.8^{+2.0}_{-2.2}$ km s^{-1} Mpc^{-1}, when combining with DESY5, Pantheon+, and Union3, respectively. We highlighted two interesting observations. The first is that even without including information from the sound horizon scale, our constraints are still in 2.2-3.0σ tension with the H_0 measurement from the SH0ES collaboration [2]. Second, we observed that our measurement is broadly consistent with other early-time H_0 measurements that *do* rely on the sound horizon scale. As discussed in section 6, some early-Universe solutions to the Hubble tension (e.g. early dark energy) may lead to deviations in sound horizon-dependent measurements of H_0, compared to those that are independent of the sound horizon scale. Therefore, we have found no significant evidence of new early-Universe physics in this work. Future data releases from DESI and other ongoing/upcoming galaxy surveys, however, will allow increasingly precise constraints on such models. It will be exciting to see how this data changes our understanding of the Hubble tension.

Acknowledgments

We thank Oliver Philcox for helpful discussions during this work, as well as Gerrit Farren for thoughtful comments on the manuscript. We additionally thank Mustapha Ishak-Boushaki and Adam Riess for their comments on the preprint version of this article.

This material is based upon work supported by the U.S. Department of Energy (DOE), Office of Science, Office of High-Energy Physics, under Contract No. DE–AC02–05CH11231, and by the National Energy Research Scientific Computing Center, a DOE Office of Science User Facility under the same contract. Additional support for DESI was provided by the U.S. National Science Foundation (NSF), Division of Astronomical Sciences under Contract No. AST-0950945 to the NSF National Optical-Infrared Astronomy Research Laboratory; the Science and Technology Facilities Council of the United Kingdom; the Gordon and Betty Moore Foundation; the Heising-Simons Foundation; the French Alternative Energies and Atomic Energy Commission (CEA); the National Council of Humanities, Science and Technology of Mexico (CONAHCYT); the Ministry of Science and Innovation of Spain (MICINN), and by the DESI Member Institutions: https://www.desi.lbl.gov/collaborating-institutions.

The DESI Legacy Imaging Surveys consist of three individual and complementary projects: the Dark Energy Camera Legacy Survey (DECaLS), the Beijing-Arizona Sky Survey (BASS), and the Mayall z-band Legacy Survey (MzLS). DECaLS, BASS and MzLS together include data obtained, respectively, at the Blanco telescope, Cerro Tololo Inter-American Observatory, NSF NOIRLab; the Bok telescope, Steward Observatory, University of Arizona; and the Mayall telescope, Kitt Peak National Observatory, NOIRLab. NOIRLab is operated by the Association of Universities for Research in Astronomy (AURA) under a cooperative agreement with the National Science Foundation. Pipeline processing and analyses of the data were supported by NOIRLab and the Lawrence Berkeley National Laboratory. Legacy Surveys also uses data products from the Near-Earth Object Wide-field Infrared Survey Explorer (NEOWISE), a project of the Jet Propulsion Laboratory/California Institute of Technology, funded by the National Aeronautics and Space Administration. Legacy Surveys was supported by: the Director, Office of Science, Office of High Energy Physics of the U.S. Department of

JCAP06(2025)020

Energy; the National Energy Research Scientific Computing Center, a DOE Office of Science User Facility; the U.S. National Science Foundation, Division of Astronomical Sciences; the National Astronomical Observatories of China, the Chinese Academy of Sciences and the Chinese National Natural Science Foundation. LBNL is managed by the Regents of the University of California under contract to the U.S. Department of Energy. The complete acknowledgments can be found at https://www.legacysurvey.org/.

Any opinions, findings, and conclusions or recommendations expressed in this material are those of the author(s) and do not necessarily reflect the views of the U.S. National Science Foundation, the U.S. Department of Energy, or any of the listed funding agencies.

The authors are honored to be permitted to conduct scientific research on Iolkam Du'ag (Kitt Peak), a mountain with particular significance to the Tohono O'odham Nation.

A Robustness tests

In this appendix we demonstrate the robustness of our results to several potential sources of systematic error. We note that unless otherwise specified, the results shown herein are obtained using emulated theoretical power spectra (see section 4.5), without the additional importance-sampling step described in section 4.6.

A.1 Sky region/imaging systematics weights

The constraints obtained in this work are derived from the broadband shape of the galaxy power spectrum, relying more on information from larger scales than in [56, 77]. This warrants special attention to the treatment of large-scale angular systematics. We test our robustness to these large-scale angular effects in two ways, with results from DESI galaxy clustering alone shown in figure 6. One one hand, we check for consistency between different regions of the sky, separately considering the data in the North and South Galactic Caps (NGC/SGC). As in [77], we compare our baseline analysis (NGC+SGC) vs. NGC alone, because the SGC region is too small to be analyzed by itself. We find very good agreement between the constraints obtained in these two regions, providing confidence in the robustness of our results. As a second test, we consider the impact of the angular systematics weights used to correct for variations in imaging (see [76] for a detailed description of this weighting). We analyze the full data (NGC+SGC) without applying any imaging weights at all, finding that the constraints obtained in this way are not significantly impacted relative to our baseline analysis, indicating that our results are robust to the choice of weighting.

A.2 Minimum k-cutoff

Motivated by similar reasoning as in the previous section, we test the impact of various choices of $k_{\rm min}$, which sets the largest scale probed by our analysis. Constraints from DESI galaxy clustering alone with $k_{\rm min} = 0.04\,h^{-1}$Mpc and $0.03\,h^{-1}$Mpc, in addition to the baseline choice of $k_{\rm min} = 0.02\,h^{-1}$Mpc, are shown in figure 7. We find that the constraints obtained are robust to the choice of $k_{\rm min}$, and thus we find no evidence of inconsistencies in the largest-scale measurements.

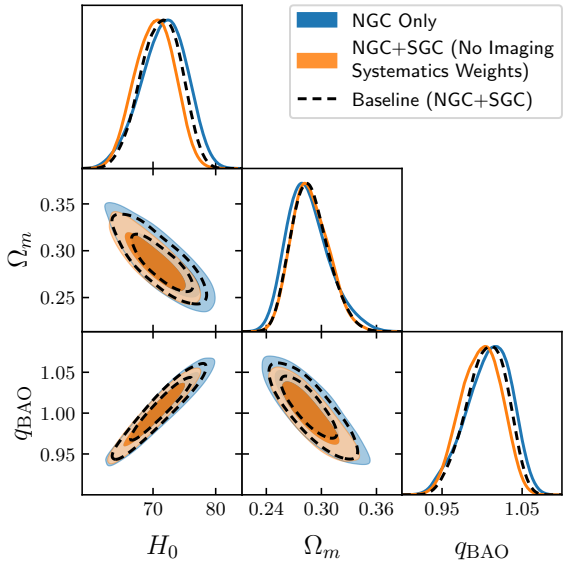

Figure 6. Constraints are shown for analysis variations designed to test our sensitivity to large-scale angular systematics. All results displayed are obtained from DESI galaxy clustering alone. The baseline results from section 5 are shown in the black dashed contours. In blue, constraints are shown for only galaxies found in the North Galactic Cap (NGC) sky region. In orange are results for the full DESI DR1 footprint (NGC+SGC), but without applying weighting to correct for imaging systematics [76]. In both cases, we find a high degree of consistency with our baseline analysis.

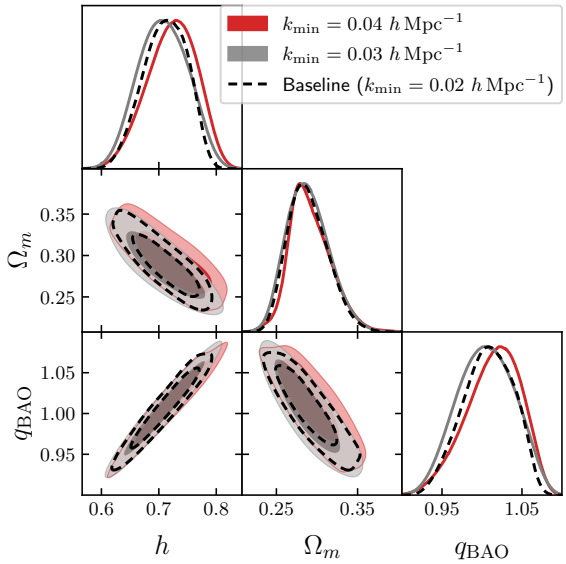

Figure 7. Constraints are shown for various choices of $k_{\rm min}$, which sets the large-scale cutoff of our analysis. Results are obtained from DESI galaxy clustering alone. The baseline results from section 5 are shown in the black dashed contours, while the gray and red contours show constraints for $k_{\rm min} = 0.03\,h^{-1}$Mpc, $0.04\,h^{-1}$Mpc respectively. We find that our results are robust to the choice of $k_{\rm min}$.

JCAP06(2025)020

Code Availability Statement. This article has associated code in a code repository. The data used in this analysis will be made public along the Data Release 1 (details in https://data.desi.lbl.gov/doc/releases/).

References

[1] E. Abdalla et al., *Cosmology intertwined: A review of the particle physics, astrophysics, and cosmology associated with the cosmological tensions and anomalies*, *JHEAp* **34** (2022) 49 [arXiv:2203.06142] [INSPIRE].

[2] A.G. Riess et al., *A Comprehensive Measurement of the Local Value of the Hubble Constant with 1 km s^{-1} Mpc^{-1} Uncertainty from the Hubble Space Telescope and the SH0ES Team*, *Astrophys. J. Lett.* **934** (2022) L7 [arXiv:2112.04510] [INSPIRE].

[3] PLANCK collaboration, *Planck 2018 results. VI. Cosmological parameters*, *Astron. Astrophys.* **641** (2020) A6 [*Erratum ibid.* **652** (2021) C4] [arXiv:1807.06209] [INSPIRE].

[4] E. Di Valentino et al., *In the realm of the Hubble tension — a review of solutions*, *Class. Quant. Grav.* **38** (2021) 153001 [arXiv:2103.01183] [INSPIRE].

[5] R. Wojtak and J. Hjorth, *Intrinsic tension in the supernova sector of the local Hubble constant measurement and its implications*, *Mon. Not. Roy. Astron. Soc.* **515** (2022) 2790 [arXiv:2206.08160] [INSPIRE].

[6] R. Wojtak and J. Hjorth, *Consistent extinction model for type Ia supernovae in Cepheid-based calibration galaxies and its impact on H_0*, *Mon. Not. Roy. Astron. Soc.* **533** (2024) 2319 [arXiv:2403.10388] [INSPIRE].

[7] C. Gall, L. Izzo, R. Wojtak and J. Hjorth, *The Hubble Constant from Blue Type Ia Supernovae*, arXiv:2411.05642 [INSPIRE].

[8] ACT collaboration, *The Atacama Cosmology Telescope: DR6 Gravitational Lensing Map and Cosmological Parameters*, *Astrophys. J.* **962** (2024) 113 [arXiv:2304.05203] [INSPIRE].

[9] BOSS collaboration, *The clustering of galaxies in the completed SDSS-III Baryon Oscillation Spectroscopic Survey: cosmological analysis of the DR12 galaxy sample*, *Mon. Not. Roy. Astron. Soc.* **470** (2017) 2617 [arXiv:1607.03155] [INSPIRE].

[10] A. Cuceu, J. Farr, P. Lemos and A. Font-Ribera, *Baryon Acoustic Oscillations and the Hubble Constant: Past, Present and Future*, *JCAP* **10** (2019) 044 [arXiv:1906.11628] [INSPIRE].

[11] DES collaboration, *Dark Energy Survey Year 3 results: A 2.7% measurement of baryon acoustic oscillation distance scale at redshift 0.835*, *Phys. Rev. D* **105** (2022) 043512 [arXiv:2107.04646] [INSPIRE].

[12] DESI collaboration, *DESI 2024 III: baryon acoustic oscillations from galaxies and quasars*, *JCAP* **04** (2025) 012 [arXiv:2404.03000] [INSPIRE].

[13] DESI collaboration, *DESI 2024 IV: Baryon Acoustic Oscillations from the Lyman alpha forest*, *JCAP* **01** (2025) 124 [arXiv:2404.03001] [INSPIRE].

[14] DESI collaboration, *DESI 2024 VI: cosmological constraints from the measurements of baryon acoustic oscillations*, *JCAP* **02** (2025) 021 [arXiv:2404.03002] [INSPIRE].

[15] W. Hu and N. Sugiyama, *Small scale cosmological perturbations: An analytic approach*, *Astrophys. J.* **471** (1996) 542 [astro-ph/9510117] [INSPIRE].

[16] D.J. Eisenstein and W. Hu, *Baryonic features in the matter transfer function*, *Astrophys. J.* **496** (1998) 605 [astro-ph/9709112] [INSPIRE].

JCAP06(2025)020

[17] L. Knox and M. Millea, *Hubble constant hunter's guide*, *Phys. Rev. D* **101** (2020) 043533 [arXiv:1908.03663] [INSPIRE].

[18] M. Doran and G. Robbers, *Early dark energy cosmologies*, *JCAP* **06** (2006) 026 [astro-ph/0601544] [INSPIRE].

[19] J. Bielefeld, W.L.K. Wu, R.R. Caldwell and O. Doré, *Freezing Out Early Dark Energy*, *Phys. Rev. D* **88** (2013) 103004 [arXiv:1305.2209] [INSPIRE].

[20] T. Karwal and M. Kamionkowski, *Dark energy at early times, the Hubble parameter, and the string axiverse*, *Phys. Rev. D* **94** (2016) 103523 [arXiv:1608.01309] [INSPIRE].

[21] D.J. Eisenstein and M.J. White, *Theoretical uncertainty in baryon oscillations*, *Phys. Rev. D* **70** (2004) 103523 [astro-ph/0407539] [INSPIRE].

[22] Z. Hou et al., *How Massless Neutrinos Affect the Cosmic Microwave Background Damping Tail*, *Phys. Rev. D* **87** (2013) 083008 [arXiv:1104.2333] [INSPIRE].

[23] F.-Y. Cyr-Racine and K. Sigurdson, *Limits on Neutrino-Neutrino Scattering in the Early Universe*, *Phys. Rev. D* **90** (2014) 123533 [arXiv:1306.1536] [INSPIRE].

[24] L. Lancaster, F.-Y. Cyr-Racine, L. Knox and Z. Pan, *A tale of two modes: Neutrino free-streaming in the early universe*, *JCAP* **07** (2017) 033 [arXiv:1704.06657] [INSPIRE].

[25] C.D. Kreisch, F.-Y. Cyr-Racine and O. Doré, *Neutrino puzzle: Anomalies, interactions, and cosmological tensions*, *Phys. Rev. D* **101** (2020) 123505 [arXiv:1902.00534] [INSPIRE].

[26] E.J. Baxter and B.D. Sherwin, *Determining the Hubble Constant without the Sound Horizon Scale: Measurements from CMB Lensing*, *Mon. Not. Roy. Astron. Soc.* **501** (2021) 1823 [arXiv:2007.04007] [INSPIRE].

[27] O.H.E. Philcox, B.D. Sherwin, G.S. Farren and E.J. Baxter, *Determining the Hubble Constant without the Sound Horizon: Measurements from Galaxy Surveys*, *Phys. Rev. D* **103** (2021) 023538 [arXiv:2008.08084] [INSPIRE].

[28] S. Brieden, H. Gil-Marín and L. Verde, *A tale of two (or more) h's*, *JCAP* **04** (2023) 023 [arXiv:2212.04522] [INSPIRE].

[29] T.L. Smith, V. Poulin and T. Simon, *Assessing the robustness of sound horizon-free determinations of the Hubble constant*, *Phys. Rev. D* **108** (2023) 103525 [arXiv:2208.12992] [INSPIRE].

[30] G.S. Farren et al., *Atacama Cosmology Telescope: Multiprobe cosmology with unWISE galaxies and ACT DR6 CMB lensing*, *Phys. Rev. D* **111** (2025) 083516 [arXiv:2409.02109] [INSPIRE].

[31] S. Das et al., *Detection of the Power Spectrum of Cosmic Microwave Background Lensing by the Atacama Cosmology Telescope*, *Phys. Rev. Lett.* **107** (2011) 021301 [arXiv:1103.2124] [INSPIRE].

[32] B.D. Sherwin et al., *Two-season Atacama Cosmology Telescope polarimeter lensing power spectrum*, *Phys. Rev. D* **95** (2017) 123529 [arXiv:1611.09753] [INSPIRE].

[33] PLANCK collaboration, *Planck 2013 results. XVII. Gravitational lensing by large-scale structure*, *Astron. Astrophys.* **571** (2014) A17 [arXiv:1303.5077] [INSPIRE].

[34] PLANCK collaboration, *Planck 2015 results. XV. Gravitational lensing*, *Astron. Astrophys.* **594** (2016) A15 [arXiv:1502.01591] [INSPIRE].

[35] PLANCK collaboration, *Planck 2018 results. VIII. Gravitational lensing*, *Astron. Astrophys.* **641** (2020) A8 [arXiv:1807.06210] [INSPIRE].

[36] J. Carron, M. Mirmelstein and A. Lewis, *CMB lensing from Planck PR4 maps*, *JCAP* **09** (2022) 039 [arXiv:2206.07773] [INSPIRE].

JCAP06(2025)020

[37] E.F. Schlafly, A.M. Meisner and G.M. Green, *The unWISE Catalog: Two Billion Infrared Sources from Five Years of WISE Imaging*, *Astrophys. J. Suppl.* **240** (2019) 30.

[38] D. Brout et al., *The Pantheon+ Analysis: Cosmological Constraints*, *Astrophys. J.* **938** (2022) 110 [arXiv:2202.04077] [INSPIRE].

[39] B. Bahr-Kalus, D. Parkinson and E.-M. Mueller, *Measurement of the matter-radiation equality scale using the extended baryon oscillation spectroscopic survey quasar sample*, *Mon. Not. Roy. Astron. Soc.* **524** (2023) 2463 [arXiv:2302.07484] [INSPIRE].

[40] F. Prada et al., *Measuring equality horizon with the zero-crossing of the galaxy correlation function*, arXiv:1111.2889 [INSPIRE].

[41] A. Krolewski, W.J. Percival and A. Woodfinden, *New Method to Determine the Hubble Parameter from Cosmological Energy-Density Measurements*, *Phys. Rev. Lett.* **134** (2025) 101002 [arXiv:2403.19227] [INSPIRE].

[42] DESI collaboration, *The DESI Experiment Part I: Science,Targeting, and Survey Design*, arXiv:1611.00036 [INSPIRE].

[43] DESI collaboration, *The DESI Experiment Part II: Instrument Design*, arXiv:1611.00037 [INSPIRE].

[44] DESI collaboration, *Validation of the Scientific Program for the Dark Energy Spectroscopic Instrument*, *Astron. J.* **167** (2024) 62 [arXiv:2306.06307] [INSPIRE].

[45] EUCLID collaboration, *Euclid. I. Overview of the Euclid mission*, *Astron. Astrophys.* **697** (2025) A1 [arXiv:2405.13491] [INSPIRE].

[46] Y. Wang et al., *The High Latitude Spectroscopic Survey on the Nancy Grace Roman Space Telescope*, *Astrophys. J.* **928** (2022) 1 [arXiv:2110.01829] [INSPIRE].

[47] SPHEREx collaboration, *Cosmology with the SPHEREX All-Sky Spectral Survey*, arXiv:1412.4872 [INSPIRE].

[48] BOSS collaboration, *The Baryon Oscillation Spectroscopic Survey of SDSS-III*, *Astron. J.* **145** (2013) 10 [arXiv:1208.0022] [INSPIRE].

[49] BOSS collaboration, *The clustering of galaxies in the completed SDSS-III Baryon Oscillation Spectroscopic Survey: baryon acoustic oscillations in the Fourier space*, *Mon. Not. Roy. Astron. Soc.* **464** (2017) 3409 [arXiv:1607.03149] [INSPIRE].

[50] G.S. Farren, O.H.E. Philcox and B.D. Sherwin, *Determining the Hubble constant without the sound horizon: Perspectives with future galaxy surveys*, *Phys. Rev. D* **105** (2022) 063503 [arXiv:2112.10749] [INSPIRE].

[51] O.H.E. Philcox et al., *Determining the Hubble constant without the sound horizon: A 3.6% constraint on H_0 from galaxy surveys, CMB lensing, and supernovae*, *Phys. Rev. D* **106** (2022) 063530 [arXiv:2204.02984] [INSPIRE].

[52] DESI collaboration, *Data Release 1 of the Dark Energy Spectroscopic Instrument*, arXiv:2503.14745 [INSPIRE].

[53] C. Alcock and B. Paczynski, *An evolution free test for non-zero cosmological constant*, *Nature* **281** (1979) 358 [INSPIRE].

[54] A. Cuceu et al., *The ap effect in the desi lyman-alpha forest* in preparation.

[55] J. Lesgourgues and S. Pastor, *Massive neutrinos and cosmology*, *Phys. Rept.* **429** (2006) 307 [astro-ph/0603494] [INSPIRE].

[56] DESI collaboration, *DESI 2024 VII: Cosmological Constraints from the Full-Shape Modeling of Clustering Measurements*, arXiv:2411.12022 [INSPIRE].

JCAP06(2025)020

[57] S. Brieden, H. Gil-Marín and L. Verde, *ShapeFit: extracting the power spectrum shape information in galaxy surveys beyond BAO and RSD*, *JCAP* **12** (2021) 054 [arXiv:2106.07641] [INSPIRE].

[58] M. Maus et al., *An analysis of parameter compression and Full-Modeling techniques with Velocileptors for DESI 2024 and beyond*, *JCAP* **01** (2025) 138 [arXiv:2404.07312] [INSPIRE].

[59] H.E. Noriega et al., *Comparing Compressed and Full-Modeling analyses with FOLPS: implications for DESI 2024 and beyond*, *JCAP* **01** (2025) 136 [arXiv:2404.07269] [INSPIRE].

[60] Y. Lai et al., *A comparison between ShapeFit compression and Full-Modelling method with PyBird for DESI 2024 and beyond*, *JCAP* **01** (2025) 139 [arXiv:2404.07283] [INSPIRE].

[61] BOSS collaboration, *Cosmological implications of baryon acoustic oscillation measurements*, *Phys. Rev. D* **92** (2015) 123516 [arXiv:1411.1074] [INSPIRE].

[62] S. Brieden, H. Gil-Marín and L. Verde, *Model-agnostic interpretation of 10 billion years of cosmic evolution traced by BOSS and eBOSS data*, *JCAP* **08** (2022) 024 [arXiv:2204.11868] [INSPIRE].

[63] W.L. Freedman et al., *Status Report on the Chicago-Carnegie Hubble Program (CCHP): Measurement of the Hubble Constant Using the Hubble and James Webb Space Telescopes*, *Astrophys. J.* **985** (2025) 203 [arXiv:2408.06153] [INSPIRE].

[64] A. Cuceu, A. Font-Ribera, B. Joachimi and S. Nadathur, *Cosmology beyond BAO from the 3D distribution of the Lyman-α forest*, *Mon. Not. Roy. Astron. Soc.* **506** (2021) 5439 [arXiv:2103.14075] [INSPIRE].

[65] A. Cuceu et al., *The Alcock-Paczyński effect from Lyman-α forest correlations: analysis validation with synthetic data*, *Mon. Not. Roy. Astron. Soc.* **523** (2023) 3773 [arXiv:2209.12931] [INSPIRE].

[66] R. Lynds, *The Absorption-Line Spectrum of 4c 05.34*, *Astrophys. J.* **164** (1971) L73.

[67] M. Rauch, *The lyman alpha forest in the spectra of quasistellar objects*, *Ann. Rev. Astron. Astrophys.* **36** (1998) 267 [astro-ph/9806286] [INSPIRE].

[68] DESI collaboration, *Overview of the Instrumentation for the Dark Energy Spectroscopic Instrument*, *Astron. J.* **164** (2022) 207 [arXiv:2205.10939] [INSPIRE].

[69] DESI collaboration, *The Robotic Multiobject Focal Plane System of the Dark Energy Spectroscopic Instrument (DESI)*, *Astron. J.* **165** (2023) 9 [arXiv:2205.09014] [INSPIRE].

[70] DESI collaboration, *The Optical Corrector for the Dark Energy Spectroscopic Instrument*, *Astron. J.* **168** (2024) 95 [arXiv:2306.06310] [INSPIRE].

[71] DESI collaboration, *The DESI Experiment, a whitepaper for Snowmass 2013*, arXiv:1308.0847 [INSPIRE].

[72] DESI collaboration, *The Spectroscopic Data Processing Pipeline for the Dark Energy Spectroscopic Instrument*, *Astron. J.* **165** (2023) 144 [arXiv:2209.14482] [INSPIRE].

[73] DESI collaboration, *Survey Operations for the Dark Energy Spectroscopic Instrument*, *Astron. J.* **166** (2023) 259 [arXiv:2306.06309] [INSPIRE].

[74] DESI collaboration, *Overview of the DESI Legacy Imaging Surveys*, *Astron. J.* **157** (2019) 168 [arXiv:1804.08657] [INSPIRE].

[75] DESI collaboration, *The Early Data Release of the Dark Energy Spectroscopic Instrument*, *Astron. J.* **168** (2024) 58 [arXiv:2306.06308] [INSPIRE].

[76] DESI collaboration, *DESI 2024 II: Sample Definitions, Characteristics, and Two-point Clustering Statistics*, arXiv:2411.12020 [INSPIRE].

JCAP06(2025)020

[77] DESI collaboration, *DESI 2024 V: Full-Shape Galaxy Clustering from Galaxies and Quasars*, arXiv:2411.12021 [INSPIRE].

[78] ACT collaboration, *The Atacama Cosmology Telescope: A Measurement of the DR6 CMB Lensing Power Spectrum and Its Implications for Structure Growth*, *Astrophys. J.* **962** (2024) 112 [arXiv:2304.05202] [INSPIRE].

[79] DES collaboration, *The Dark Energy Survey: Cosmology Results with ∼1500 New High-redshift Type Ia Supernovae Using the Full 5 yr Data Set*, *Astrophys. J. Lett.* **973** (2024) L14 [arXiv:2401.02929] [INSPIRE].

[80] D. Scolnic et al., *The Pantheon+ Analysis: The Full Data Set and Light-curve Release*, *Astrophys. J.* **938** (2022) 113 [arXiv:2112.03863] [INSPIRE].

[81] D. Rubin et al., *Union Through UNITY: Cosmology with 2,000 SNe Using a Unified Bayesian Framework*, arXiv:2311.12098 [INSPIRE].

[82] M. Pinon et al., *Mitigation of DESI fiber assignment incompleteness effect on two-point clustering with small angular scale truncated estimators*, *JCAP* **01** (2025) 131 [arXiv:2406.04804] [INSPIRE].

[83] A. de Mattia and V. Ruhlmann-Kleider, *Integral constraints in spectroscopic surveys*, *JCAP* **08** (2019) 036 [arXiv:1904.08851] [INSPIRE].

[84] D. Forero-Sánchez et al., *Analytical and EZmock covariance validation for the DESI 2024 results*, *JCAP* **04** (2025) 055 [arXiv:2411.12027] [INSPIRE].

[85] C.-H. Chuang et al., *EZmocks: extending the Zel'dovich approximation to generate mock galaxy catalogues with accurate clustering statistics*, *Mon. Not. Roy. Astron. Soc.* **446** (2015) 2621 [arXiv:1409.1124] [INSPIRE].

[86] S.-F. Chen, Z. Vlah and M. White, *Consistent Modeling of Velocity Statistics and Redshift-Space Distortions in One-Loop Perturbation Theory*, *JCAP* **07** (2020) 062 [arXiv:2005.00523] [INSPIRE].

[87] S.-F. Chen, Z. Vlah, E. Castorina and M. White, *Redshift-Space Distortions in Lagrangian Perturbation Theory*, *JCAP* **03** (2021) 100 [arXiv:2012.04636] [INSPIRE].

[88] H. Jeffreys, *An invariant form for the prior probability in estimation problems*, *Proc. Roy. Soc. Lond. A* **186** (1946) 453.

[89] B. Hadzhiyska et al., *Cosmology with 6 parameters in the Stage-IV era: efficient marginalisation over nuisance parameters*, arXiv:2301.11895 [DOI:10.21105/astro.2301.11895] [INSPIRE].

[90] KATRIN collaboration, *Direct neutrino-mass measurement with sub-electronvolt sensitivity*, *Nature Phys.* **18** (2022) 160 [arXiv:2105.08533] [INSPIRE].

[91] N. Schöneberg, *The 2024 BBN baryon abundance update*, *JCAP* **06** (2024) 006 [arXiv:2401.15054] [INSPIRE].

[92] T. Simon, P. Zhang, V. Poulin and T.L. Smith, *Consistency of effective field theory analyses of the BOSS power spectrum*, *Phys. Rev. D* **107** (2023) 123530 [arXiv:2208.05929] [INSPIRE].

[93] E.B. Holm et al., *Bayesian and frequentist investigation of prior effects in EFT of LSS analyses of full-shape BOSS and eBOSS data*, *Phys. Rev. D* **108** (2023) 123514 [arXiv:2309.04468] [INSPIRE].

[94] C. Robert and G. Casella, *Monte Carlo statistical methods*, Springer Verlag (2004).

[95] M.D. Hoffman and A. Gelman, *The No-U-Turn Sampler: Adaptively Setting Path Lengths in Hamiltonian Monte Carlo*, *J. Machine Learning Res.* **15** (2014) 1593 [arXiv:1111.4246] [INSPIRE].

JCAP06(2025)020

[96] S.P. Brooks and A. Gelman, *General Methods for Monitoring Convergence of Iterative Simulations*, *J. Comput. Graphical Stat.* **7** (1998) 434.

[97] N.A. Maksimova et al., *AbacusSummit: a massive set of high-accuracy, high-resolution N-body simulations*, *Mon. Not. Roy. Astron. Soc.* **508** (2021) 4017 [arXiv:2110.11398] [INSPIRE].

[98] L.H. Garrison, D.J. Eisenstein and P.A. Pinto, *A High-Fidelity Realization of the Euclid Code Comparison N-body Simulation with Abacus*, *Mon. Not. Roy. Astron. Soc.* **485** (2019) 3370 [arXiv:1810.02916] [INSPIRE].

[99] S. Yuan et al., *The DESI one-per cent survey: exploring the halo occupation distribution of luminous red galaxies and quasi-stellar objects with AbacusSummit*, *Mon. Not. Roy. Astron. Soc.* **530** (2024) 947 [arXiv:2306.06314] [INSPIRE].

[100] A. Rocher et al., *The DESI One-Percent survey: exploring the Halo Occupation Distribution of Emission Line Galaxies with AbacusSummit simulations*, *JCAP* **10** (2023) 016 [arXiv:2306.06319] [INSPIRE].

[101] A. Smith et al., *Generating mock galaxy catalogues for flux-limited samples like the DESI Bright Galaxy Survey*, *Mon. Not. Roy. Astron. Soc.* **532** (2024) 903 [arXiv:2312.08792] [INSPIRE].

[102] M.M.S. Hanif et al., *Fast Fiber Assign: Emulating fiber assignment effects for realistic DESI catalogs*, in preparation.

[103] DESI collaboration, *Production of alternate realizations of DESI fiber assignment for unbiased clustering measurement in data and simulations*, *JCAP* **01** (2025) 127 [arXiv:2404.03006] [INSPIRE].

[104] P.L. Taylor and K. Markovič, *Covariance of photometric and spectroscopic two-point statistics: Implications for cosmological parameter inference*, *Phys. Rev. D* **106** (2022) 063536 [arXiv:2205.14167] [INSPIRE].

[105] P.L. Taylor, A. Cuceu, C.-H. To and E.A. Zaborowski, *CombineHarvesterFlow: Joint Probe Analysis Made Easy with Normalizing Flows*, arXiv:2406.06687 [DOI:10.33232/001c.124495] [INSPIRE].

[106] M. Raveri and C. Doux, *Non-Gaussian estimates of tensions in cosmological parameters*, *Phys. Rev. D* **104** (2021) 043504 [arXiv:2105.03324] [INSPIRE].

[107] SDSS collaboration, *The Sloan Digital Sky Survey: Technical Summary*, *Astron. J.* **120** (2000) 1579 [astro-ph/0006396] [INSPIRE].

[108] A.G. Riess et al., *JWST Validates HST Distance Measurements: Selection of Supernova Subsample Explains Differences in JWST Estimates of Local H_0*, *Astrophys. J.* **977** (2024) 120 [arXiv:2408.11770] [INSPIRE].

[109] T.L. Smith, V. Poulin and M.A. Amin, *Oscillating scalar fields and the Hubble tension: a resolution with novel signatures*, *Phys. Rev. D* **101** (2020) 063523 [arXiv:1908.06995] [INSPIRE].

[110] J.C. Hill et al., *Atacama Cosmology Telescope: Constraints on prerecombination early dark energy*, *Phys. Rev. D* **105** (2022) 123536 [arXiv:2109.04451] [INSPIRE].

JCAP06(2025)020

Author List

E.A. Zaborowski[1,2,3], P. Taylor[3], K. Honscheid[1,2,3], A. Cuceu[4], A. de Mattia[5], D. Huterer[6,7], A. Krolewski[8,9,10], P. Martini[1,11,3], A.J. Ross[1,11,3], C. To[3], A. Torres[3], S. Ahlen[12], D. Bianchi[13], D. Brooks[14], E. Buckley-Geer[15,16], E. Burtin[5], T. Claybaugh[4], S. Cole[17], A. de la Macorra[18], Arjun Dey[19], Biprateep Dey[20,21], P. Doel[14], S. Ferraro[4,22], A. Font-Ribera[14,23], J.E. Forero-Romero[24,25], E. Gaztañaga[26,27,28], H. Gil-Marín[29,26,30], G. Gutierrez[16], J. Guy[4], C. Hahn[31], C. Howlett[32], S. Juneau[19], R. Kehoe[33], D. Kirkby[34], T. Kisner[4], A. Kremin[4], M. Landriau[4], L. Le Guillou[35], M.E. Levi[4], C. Magneville[5], A. Meisner[19], R. Miquel[36,23], J. Moustakas[37], N. Palanque-Delabrouille[5,4], W.J. Percival[8,9,10], F. Prada[38], I. Pérez-Ràfols[39], G. Rossi[40], E. Sanchez[41], D. Schlegel[4], M. Schubnell[6,7], H. Seo[42], D. Sprayberry[19], G. Tarlé[7], B.A. Weaver[19], R.H. Wechsler[43,44,45]

[1] *Center for Cosmology and AstroParticle Physics, The Ohio State University, 191 West Woodruff Avenue, Columbus, OH 43210, U.S.A.*
[2] *Department of Physics, The Ohio State University, 191 West Woodruff Avenue, Columbus, OH 43210, U.S.A.*
[3] *The Ohio State University, Columbus, 43210 OH, U.S.A.*
[4] *Lawrence Berkeley National Laboratory, 1 Cyclotron Road, Berkeley, CA 94720, U.S.A.*
[5] *IRFU, CEA, Université Paris-Saclay, F-91191 Gif-sur-Yvette, France*
[6] *Department of Physics, University of Michigan, Ann Arbor, MI 48109, U.S.A.*
[7] *University of Michigan, Ann Arbor, MI 48109, U.S.A.*
[8] *Department of Physics and Astronomy, University of Waterloo, 200 University Ave W, Waterloo, ON N2L 3G1, Canada*
[9] *Perimeter Institute for Theoretical Physics, 31 Caroline St. North, Waterloo, ON N2L 2Y5, Canada*
[10] *Waterloo Centre for Astrophysics, University of Waterloo, 200 University Ave W, Waterloo, ON N2L 3G1, Canada*
[11] *Department of Astronomy, The Ohio State University, 4055 McPherson Laboratory, 140 W 18th Avenue, Columbus, OH 43210, U.S.A.*
[12] *Physics Dept., Boston University, 590 Commonwealth Avenue, Boston, MA 02215, U.S.A.*
[13] *Dipartimento di Fisica "Aldo Pontremoli", Università degli Studi di Milano, Via Celoria 16, I-20133 Milano, Italy*
[14] *Department of Physics & Astronomy, University College London, Gower Street, London, WC1E 6BT, U.K.*
[15] *Department of Astronomy and Astrophysics, University of Chicago, 5640 South Ellis Avenue, Chicago, IL 60637, U.S.A.*
[16] *Fermi National Accelerator Laboratory, PO Box 500, Batavia, IL 60510, U.S.A.*
[17] *Institute for Computational Cosmology, Department of Physics, Durham University, South Road, Durham DH1 3LE, U.K.*
[18] *Instituto de Física, Universidad Nacional Autónoma de México, Circuito de la Investigación Científica, Ciudad Universitaria, Cd. de México C. P. 04510, Mexico*
[19] *NSF NOIRLab, 950 N. Cherry Ave., Tucson, AZ 85719, U.S.A.*
[20] *Department of Astronomy & Astrophysics, University of Toronto, Toronto, ON M5S 3H4, Canada*

JCAP06(2025)020

[21] *Department of Physics & Astronomy and Pittsburgh Particle Physics, Astrophysics, and Cosmology Center (PITT PACC), University of Pittsburgh, 3941 O'Hara Street, Pittsburgh, PA 15260, U.S.A.*
[22] *University of California, Berkeley, 110 Sproul Hall #5800 Berkeley, CA 94720, U.S.A.*
[23] *Institut de Física d'Altes Energies (IFAE), The Barcelona Institute of Science and Technology, Campus UAB, 08193 Bellaterra Barcelona, Spain*
[24] *Departamento de Física, Universidad de los Andes, Cra. 1 No. 18A-10, Edificio Ip, CP 111711, Bogotá, Colombia*
[25] *Observatorio Astronómico, Universidad de los Andes, Cra. 1 No. 18A-10, Edificio H, CP 111711 Bogotá, Colombia*
[26] *Institut d'Estudis Espacials de Catalunya (IEEC), 08034 Barcelona, Spain*
[27] *Institute of Cosmology and Gravitation, University of Portsmouth, Dennis Sciama Building, Portsmouth, PO1 3FX, U.K.*
[28] *Institute of Space Sciences, ICE-CSIC, Campus UAB, Carrer de Can Magrans s/n, 08913 Bellaterra, Barcelona, Spain*
[29] *Departament de Física Quàntica i Astrofísica, Universitat de Barcelona, Martí i Franquès 1, E08028 Barcelona, Spain*
[30] *Institut de Ciències del Cosmos (ICCUB), Universitat de Barcelona (UB), c. Martí i Franquès, 1, 08028 Barcelona, Spain*
[31] *Department of Astrophysical Sciences, Princeton University, Princeton NJ 08544, U.S.A.*
[32] *School of Mathematics and Physics, University of Queensland, 4072, Australia*
[33] *Department of Physics, Southern Methodist University, 3215 Daniel Avenue, Dallas, TX 75275, U.S.A.*
[34] *Department of Physics and Astronomy, University of California, Irvine, 92697, U.S.A.*
[35] *Sorbonne Université, CNRS/IN2P3, Laboratoire de Physique Nucléaire et de Hautes Energies (LPNHE), FR-75005 Paris, France*
[36] *Institució Catalana de Recerca i Estudis Avançats, Passeig de Lluís Companys, 23, 08010 Barcelona, Spain*
[37] *Department of Physics and Astronomy, Siena College, 515 Loudon Road, Loudonville, NY 12211, U.S.A.*
[38] *Instituto de Astrofísica de Andalucía (CSIC), Glorieta de la Astronomía, s/n, E-18008 Granada, Spain*
[39] *Departament de Física, EEBE, Universitat Politècnica de Catalunya, c/Eduard Maristany 10, 08930 Barcelona, Spain*
[40] *Department of Physics and Astronomy, Sejong University, Seoul, 143-747, Korea*
[41] *CIEMAT, Avenida Complutense 40, E-28040 Madrid, Spain*
[42] *Department of Physics & Astronomy, Ohio University, Athens, OH 45701, U.S.A.*
[43] *Kavli Institute for Particle Astrophysics and Cosmology, Stanford University, Menlo Park, CA 94305, U.S.A.*
[44] *Physics Department, Stanford University, Stanford, CA 93405, U.S.A.*
[45] *SLAC National Accelerator Laboratory, Menlo Park, CA 94305, U.S.A.*

JCAP06(2025)020